Article

Dimensional Effects on the LO–TO Splitting in CF: First-Principles and Infrared Absorption Studies

Wai-Leung Yim, Oleg Byl, John T. Yates,, and J. Karl Johnson

J. Am. Chem. Soc., **2005**, 127 (9), 3198-3206• DOI: 10.1021/ja043540v • Publication Date (Web): 10 February 2005

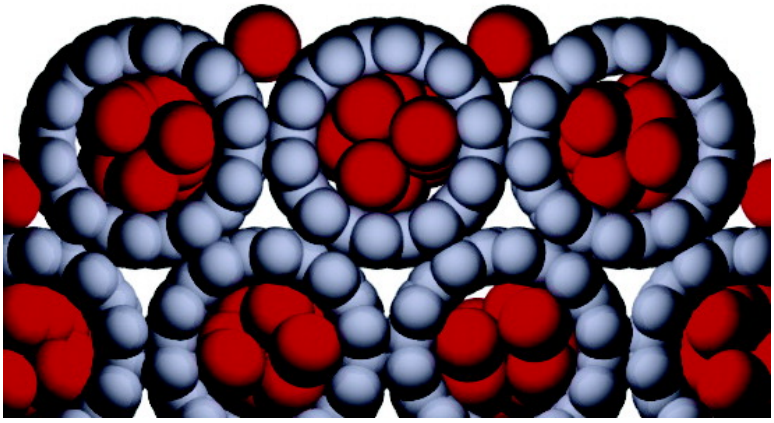

J|A|C|S
ARTICLES
Published on Web 02/10/2005

Dimensional Effects on the LO−TO Splitting in CF_4: First-Principles and Infrared Absorption Studies

Wai-Leung Yim,[†,‡] Oleg Byl,[‡] John T. Yates, Jr.,[‡] and J. Karl Johnson*[,†,§]

Contribution from the Department of Chemical Engineering, University of Pittsburgh, Pittsburgh, Pennsylvania 15261, Department of Chemistry, Surface Science Center, University of Pittsburgh, Pittsburgh, Pennsylvania 15260, and National Energy Technology Laboratory, United States Department of Energy, Pittsburgh, Pennsylvania 15236

Received October 25, 2004; E-mail: karlj@pitt.edu

Abstract: The development of longitudinal optical−transverse optical (LO−TO) modes in CF_4 has been studied experimentally and theoretically as a function of dimensionality. Infrared absorption experiments for CF_4 adsorbed on single-walled carbon nanotubes indicate a lack of LO−TO splitting at low coverage and a gradual appearance of LO−TO modes as the coverage of CF_4 on the nanotubes is increased. We have performed density functional perturbation theory calculations for the vibrational frequencies, IR absorption spectra, and phonon density of states for CF_4 in one, two, and three dimensions. The calculations demonstrate that LO−TO splitting in 1D is qualitatively different from that computed for 2D or the bulk. The magnitude of the splitting in 1D is about one-half that computed for the bulk, and the LO mode is very weakly blue-shifted in 1D. We predict that the phonon density of states changes dramatically as the dimensionality of the crystal is changed. This prediction can be tested experimentally via inelastic neutron scattering. We conclude that LO−TO splitting can be used as a probe to identify 1D states of matter.

I. Introduction

The study of one-dimensional (1D) states of matter has recently enjoyed a significant burst of activity thanks to the discovery of single-walled carbon nanotubes (SWNTs).[1−12] SWNTs are 1D structures constructed by rolling a single graphene sheet into a tube. The diameters of SWNTs are typically on the order of 1 nm, while the lengths can be many micrometers.[13,14] SWNTs are known to self-assemble on to a 2D hexagonal lattice to form bundles containing tens to hundreds of individual tubes. Perfectly packed bundles of SWNTs provide three possible sites for gas adsorption that could result in an effective 1D state of matter. These sites are the interior of the nanotube (endohedral site), the interstitial channel (formed where three tubes meet), and the exterior groove site (formed where two tubes meet on the surface of the bundle). There is evidence for simple gases adsorbing in 1D groove and endohedrial sites.[5,9,10,12,15−27] However, there is little direct evidence of how the 1D environment affects the properties of the adsorbed gas.[28,29]

We have recently studied the adsorption of CF_4 on SWNT bundles through a combination of experimental IR and molecular modeling.[19] CF_4 has an intense IR absorption peak at 1281 cm^{-1} for the ν_3 asymmetric stretching mode. In the IR spectrum

† Department of Chemical Engineering, University of Pittsburgh.
‡ Department of Chemistry, University of Pittsburgh.
§ United States Department of Energy.

(1) Graim, T.; Landau, D. P. *Phys. Rev. B* **1981**, *24*, 5156.
(2) Stan, G.; Crespi, V. H.; Cole, M. W.; Boninsegni, M. *J. Low Temp. Phys.* **1998**, *113*, 447.
(3) Calbi, M. M.; Gatica, S. M.; Bojan, M. J.; Cole, M. W. *J. Chem. Phys.* **2001**, *115*, 9975.
(4) Gatica, S. M.; Bojan, M. J.; Stan, G.; Cole, M. W. *J. Chem. Phys.* **2001**, *114*, 3765.
(5) Talapatra, S.; Migone, A. D. *Phys. Rev. Lett.* **2001**, *87*, 206106.
(6) Cole, M. W.; Crespi, V. H.; Stan, G.; Ebner, C.; Hartman, J. M.; Moroni, S.; Boninsegni, M. *Phys. Rev. Lett.* **2000**, *84*, 3883.
(7) Gordillo, M. C.; Boronat, J.; Casulleras, J. *Phys. Rev. Lett.* **2000**, *85*, 2348.
(8) Gordillo, M. C.; Boronat, J.; Casulleras, J. *Phys. Rev. B* **2000**, *61*, R878.
(9) Teizer, W.; Hallock, R. B.; Dujardin, E.; Ebbesen, T. W. *Phys. Rev. Lett.* **1999**, *82*, 5305.
(10) Talapatra, S.; Krungleviciute, V.; Migone, A. D. *Phys. Rev. Lett.* **2002**, *89*, 246106.
(11) Talapatra, S.; Migone, A. D. *Phys. Rev. B* **2002**, *65*, 045416.
(12) Wilson, T.; Vilches, O. E. *Low Temp. Phys.* **2003**, *29*, 732.
(13) Dai, H.; Hafner, J. H.; Rinzler, A. G.; Colbert, D. T.; Smalley, R. E. *Nature* **1996**, *384*, 147.
(14) Kong, J.; Soh, H. T.; Cassell, A. M.; Quate, C. F.; Dai, H. *Nature* **1998**, *395*, 878.
(15) Kuznetsova, A.; Mawhinney, D. B.; Naumenko, V.; Yates, J. T., Jr.; Liu, J.; Smalley, R. E. *Chem. Phys. Lett.* **2000**, *321*, 292.
(16) Kuznetsova, A.; Yates, J. T., Jr.; Liu, J.; Smalley, R. E. *J. Chem. Phys.* **2000**, *112*, 9590.
(17) Kuznetsova, A.; Yates, J. T., Jr.; Simonyan, V. V.; Johnson, J. K.; Huffman, C. B.; Smalley, R. E. *J. Chem. Phys.* **2001**, *115*, 6691.
(18) Byl, O.; Kondratyuk, P.; Yates, J. T., Jr. *J. Phys. Chem. B* **2003**, *107*, 4277.
(19) Byl, O.; Kondratyuk, P.; Forth, S. T.; FitzGerald, S. A.; Chen, L.; Johnson, J. K.; Yates, J. T., Jr. *J. Am. Chem. Soc.* **2003**, *125*, 5889.
(20) Weber, S. E.; Talapatra, S.; Journet, C.; Zambano, A.; Migone, A. D. *Phys. Rev. B* **2000**, *61*, 13150.
(21) Talapatra, S.; Zambano, A. Z.; Weber, S. E.; Migone, A. D. *Phys. Rev. Lett.* **2000**, *85*, 138.
(22) Muris, M.; Dupont-Pavlovsky, N.; Bienfait, M.; Zeppenfeld, P. *Surf. Sci.* **2001**, *492*, 67.
(23) Wilson, T.; Tyburski, A.; DePies, M. R.; Vilches, O. E.; Becquet, D.; Bienfait, M. *J. Low Temp. Phys.* **2002**, *126*, 403.
(24) Weber, S. E.; Talapatra, S.; Journet, C.; Zambano, A.; Migone, A. D. *Phys. Rev. B* **2002**, *66*, 49901.
(25) Ulbricht, H.; Kriebel, J.; Moos, G.; Hertel, T. *Chem. Phys. Lett.* **2002**, *363*, 252.
(26) Wilson, T.; Vilches, O. E. *Physica B* **2003**, *329*, 278.
(27) Bienfait, M.; Zeppenfeld, P.; Dupont-Pavlovsky, N.; Muris, M.; Johnson, M. R.; Wilson, T.; DePies, M.; Vilches, O. E. *Phys. Rev. B* **2004**, *70*, 35410.
(28) Lasjaunias, J. C.; Biljakovic, K.; Sauvajol, J. L.; Monceau, P. *Phys. Rev. Lett.* **2003**, *91*, 25901.
(29) Ramachandran, S.; Wilson, T. A.; Vandervelde, D.; Holmes, D. K.; Vilches, O. E. *J. Low Temp. Phys.* **2004**, *134*, 115.

 10.1021/ja043540v CCC: $30.25

of liquid CF_4, the absorption peak of the ν_3 mode is split into a doublet separated by about 70 cm^{-1}. This splitting is due to dynamic dipole interaction. There is a large electronegativity difference between carbon and fluorine that generates a considerable dynamic dipole resulting from the distortion of the CF_4 tetrahedron. This dynamic dipole in turn interacts with the neighboring CF_4 molecules and perturbs their vibrational frequencies. This phenomenon is analogous to the longitudinal optical−transverse optical (LO−TO) splitting in ionic crystals, for example, NaCl, where the LO mode leads to a blue-shift in the vibrational frequency, while the TO mode leads to a red-shift. LO−TO splitting of CF_4 has been previously studied in the bulk[30−33] and on the surface of ice.[34,35]

Our previous experimental IR study failed to find any evidence of LO−TO splitting for CF_4 adsorbed on SWNT bundles.[19] It is not clear from the experiments whether the absence of LO−TO splitting is due to the low concentration of CF_4 adsorbed on the SWNTs or due to the one-dimensional nature of the phonon modes of CF_4 adsorbed inside the SWNTs and in the groove sites. Atomistic simulations of adsorption at the experimental temperature of 133 K and pressure of 0.033 Torr predicted that the CF_4 density inside the SWNTs would be close to that of liquid CF_4,[19] implying that CF_4 concentration is not the reason for the absence of LO−TO splitting. It is therefore interesting to ask whether the absence of LO−TO splitting for CF_4 adsorbed on SWNTs is a signature of the 1D nature of the adsorbed phase.

In this work, we have studied LO−TO splitting both theoretically and experimentally. We have used density functional theory (DFT) to study the lattice dynamics and IR absorption of CF_4, varying both the dimensionality and the concentration of the CF_4 phase. We have experimentally measured the IR spectra of CF_4 adsorbed on SWNTs as a function of coverage. The combined theoretical and experimental studies give a detailed picture of the development of LO−TO splitting as the concentration of the adsorbed gas is increased.

Previous work indicates that CF_4 preferentially adsorbs in the groove and the internal sites at low coverage.[19] The groove sites allow only a 1D line of CF_4 molecules to adsorb at low coverage, with the molecules confined by the strong solid−fluid potential of the groove site. The CF_4 molecules adsorbed inside the nanotubes are not confined to a line, but are adsorbed against the inside walls of the nanotubes, forming a quasi-1D environment. At higher CF_4 coverage, multilayers of CF_4 appear on the external surface of the nanotubes, giving rise to a bulklike phase. We have experimentally probed a wide range of coverages of CF_4 on SWNTs through control of the temperature and pressure of the system. We find that LO−TO splitting is clearly observed from IR experiments at higher coverages, while LO−TO splitting cannot be observed experimentally at low coverages. Our DFT calculations address the issue of whether LO−TO splitting can occur in 1D and quasi-1D environments.

II. Computational Methods

We have performed three types of calculations relating to the IR spectra of CF_4.

First, we have computed the vibrational frequencies of CF_4 for bulk, gas phase, 1D chains, and CF_4 adsorbed on SWNTs from the direct force constant approach using VASP.[36−38] Second, we have computed IR intensities (absorption) from density functional perturbation theory (DFPT) using the PWscf package[39] combined with the method of Balan and co-workers.[40] Last, we have computed the phonon density of states (PDOSs) and their corresponding dispersion relations in the first Brillouin zone from DFPT using PWscf. All calculations utilized the nonrelativistic local density approximation (LDA). This level of theory was used previously by us to study the vibrational modes of CO_2 on SWNTs.[41] The DFPT calculations were carried out for CF_4 in the 3D bulk solid, the 2D solid consisting of one, two, and three layers, and 1D chains. The effect of the nanotubes was not explicitly included in the DFPT calculations.

A. Vibrational Frequency of Adsorbed CF_4 in the Groove Site and Internal Adsorption Site. We have carried out VASP calculations using Vanderbilt's ultrasoft pseudopotentials (USPP).[42] In the following sections, the results computed using VASP are denoted by LDA/USPP. The cutoff energies for the wave function and augmentation charge were set to 424.5 and 975.2 eV, respectively. The vibrational frequencies were calculated by the direct force constant approach.[43] Calculations were performed for CF_4 on metallic (10,10) and semiconducting (17,0) SWNTs, in the groove site and interior of the nanotube. These two types of SWNTs have diameters similar to those observed for SWNTs produced by laser ablation.[44]

Adsorption of CF_4 on the metallic (10,10) SWNTs was simulated using a supercell having two primitive unit cells of the (10,10) SWNT, giving a supercell length of 4.9 Å. For CF_4 inside the (10,10) SWNT, CF_4 and SWNT are put into a hexagonal cell of 22.1 Å × 21.9 Å × 4.9 Å, giving a separation between the adjacent tubes of about 8.4 Å. For the CF_4 in the groove site, a rectangular supercell of 16.3 Å × 24.3 Å × 4.9 Å was used. One primitive unit cell was used for the (17,0) nanotube, giving a supercell length of 4.2 Å. Internal adsorption in the (17,0) SWNT used a hexagonal cell of 22.3 Å × 22.3 Å × 4.2 Å. Groove site adsorption used a rectangular supercell of 16.3 Å × 24.3 Å × 4.2 Å. The k-space integration used 1 × 1 × 6 **k** meshes in all cases.

The vibrational frequency of gas-phase CF_4 at the Γ point was calculated using LDA/USPP. The gas phase was approximated by placing a single molecule into a cubic box 15.0 Å on a side.

B. Phonon Calculations for CF_4 in Different Dimensionalities. The PWscf calculations used norm-conserving pseudopotentials generated by the Troullier−Martins scheme[45] for carbon and fluorine atoms, using the fhi98PP pseudopotential package.[46] A high cutoff energy of 80 Ry was chosen for the pseudopotentials. The k-space integration used 3 × 3 × 3 **k** meshes for 3D and 1D models, and 3 × 3 × 1 **k** meshes for 2D slab models. The LDA PWscf calculations are denoted by LDA/NCPP in the following sections.

We have modeled orientationally ordered structures of CF_4 to reduce the computational demands in the DFT and DFPT calculations. It is

(30) Fournier, R. P.; Savoie, R.; Bessette, F.; Cabana, A. *J. Chem. Phys.* **1968**, *49*, 1159.
(31) Yvinec, M.; Pick, R. M. *J. Chem. Phys.* **1979**, *71*, 3440.
(32) Gilbert, M.; Drifford, M. *J. Chem. Phys.* **1977**, *66*, 3205.
(33) Nectoux, P.; Drifford, M.; Belloni, L.; Vinit, A. *Mol. Phys.* **1983**, *49*, 1375.
(34) Buch, V.; Delzeit, L.; Blackledge, C.; Devlin, J. P. *J. Phys. Chem.* **1996**, *100*, 3732.
(35) Delzeit, L.; Devlin, M. S.; Rowland, B.; Devlin, J. P.; Buch, V. *J. Phys. Chem.* **1996**, *100*, 10076.
(36) Kresse, G.; Hafner, J. *Phys. Rev. B* **1993**, *47*, 558.
(37) Kresse, G.; Hafner, J. *Phys. Rev. B* **1994**, *49*, 14251.
(38) Kresse, G.; Furthmueller, J. *Phys. Rev. B* **1996**, *54*, 11169.
(39) Baroni, S.; Corso, A. D.; Gironcoli, S. d.; Giannozzi, P. 2003, http://www.pwscf.org.
(40) Balan, E.; Saitta, A. M.; Mauri, F.; Calas, G. *Am. Mineral.* **2001**, *86*, 1321.
(41) Yim, W.-L.; Byl, O.; Yates, J. T., Jr.; Johnson, J. K. *J. Chem. Phys.* **2004**, *120*, 5377.
(42) Vanderbilt, D. *Phys. Rev. B* **1990**, *41*, 7892.
(43) Morrison, I.; Li, J. C.; Jenkins, S.; Xantheas, S. S.; Payne, M. C. *J. Phys. Chem. B* **1997**, *101*, 6146.
(44) Thess, A.; Lee, R.; Nikolaev, P.; Dai, H.; Petit, P.; Robert, J.; Xu, C.; Lee, Y. H.; Kim, S. G.; Rinzler, A. G.; Colbert, D. T.; Scuseria, G. E.; Tománek, D.; Fischer, J. E.; Smalley, R. E. *Science* **1996**, *273*, 483.
(45) Troullier, N.; Martins, J. L. *Phys. Rev. B* **1991**, *43*, 1993.
(46) Fuchs, M.; Scheffler, M. *Comput. Phys. Commun.* **1999**, *119*, 67.

Table 1. Vibrational Frequencies of Gas-Phase CF_4

vibrational mode[a]	ν_1	ν_2	ν_3	ν_4
degeneracy	1	2	3	3
LSDA/6-31G[b]			1264	573
LDA/NCPP[c]	884	407	1218	597
LDA/USPP[d]	908	423	1238	611
experiment[e]	909	435	1281	632

[a] ν_1 = symmetric stretching; ν_2 = symmetric bending; ν_3 = asymmetric stretching; ν_4 = asymmetric bending. [b] LDA calculations of Byl et al.[19] [c] This work, calculated from PWscf. [d] This work, calculated from VASP. [e] Previous experimental work of Byl et al.[19]

known that orientational disordering broadens the LO and TO bands without greatly affecting the overall splitting patterns.[31,32] The crystal structure of the CF_4 solid in phase II (orientationally ordered) has four CF_4 molecules per unit cell with space group $C2/c$.[47] LDA calculations show a potential minimum with a^*/a_0 at 0.95, where a^* is the optimized lattice parameter and a_0 is the experimental result. This 5% discrepancy is in the acceptable range, when compared to the previous LDA calculations for the Xe crystal, which had 4% deviation in lattice parameters from experimental results.[48] We note that most functionals used in DFT cannot account accurately for weak interactions that are due to electron correlation.[49−54] New methods have been developed to deal with van der Waals interactions within DFT.[51,55−59] However, we use the LDA formalism because it has been shown to be reasonably accurate for selected cases involving graphene systems.[60,61] We expect LO−TO splitting to be described relatively well by LDA because the dynamic dipole interactions are mainly electrostatic in nature, which can be treated by LDA relatively accurately.

We have also considered CF_4 molecules in a body-centered cubic (bcc) cell, to study the space group effect on the LO−TO splitting. It is reasonable to choose a bcc Bravais lattice for CF_4, because SiF_4, a larger group IV tetrafluoride, packs in a bcc lattice.[62,63]

The gas-phase CF_4 was modeled within LDA/NCPP using a single CF_4 molecule in a bcc cell. Γ point sampling in **k** space integration was used. The length of the lattice vector was set to 20.0 Å, which was long enough to avoid intermolecular interactions.

Gas-phase vibrational frequencies for CF_4 computed from various methods are shown in Table 1, along with the experimental frequencies. LDA calculations universally underestimate the vibrational frequencies of the different modes as compared to experiment. However, we are interested in shifts of the frequencies rather than absolute values. We expect the qualitative trends to be accurate, although the absolute frequencies are underestimated.

C. IR Absorption Calculations for CF_4 in Different Dimensionalities. The coupling between an incident radiation wave vector and the phonon wave vector of a solid is only effective when $\boldsymbol{k} \approx \boldsymbol{q}$, where $\boldsymbol{k}$ is the radiation wave vector and $\boldsymbol{q}$ is the phonon wave vector. Because the IR wavelength is much longer than the lattice constants, IR absorption occurs when $\boldsymbol{k} = \boldsymbol{q} \rightarrow 0$. In this work, we employed the method of Balan et al.[40] to calculate the IR spectra of condensed CF_4 for $q \rightarrow 0$. The average adsorbed power is given by

$$W(\omega) \propto \omega \, \mathrm{Im}[\epsilon(\omega)] \qquad (1)$$

where ω is the frequency, and $\epsilon(\omega)$ is $^1/_3$ of the trace of $\overleftrightarrow{\epsilon}(\omega)$, the dielectric tensor of the sample. The low-frequency dielectric tensor $\overleftrightarrow{\epsilon}(\omega)$ can be calculated by using the vibrational frequencies and Born effective charge tensors,[64] which were obtained from the DFPT method.

III. Experimental Section

Purified SWNTs produced by the laser vaporization method were used in this study. The same batch of nanotubes was used in our earlier experiments, and a detailed characterization of the sample can be found elsewhere.[15−17,19,65]

A sample of SWNTs was deposited from a DMF suspension onto one of two CaF_2 supporting spots pressed into a tungsten grid. The second CaF_2 spot was used as a reference. The tungsten grid was connected to massive Ni clamps fastened to Cu wires that served as power leads and provided thermal contact with the refrigerant. The sample temperature was controlled by an alumel−chromel thermocouple welded to the top of the grid. The nanotubes were ozonized at 303 K in three cycles, lasting 5 min each. The initial O_3 pressures were 21.8, 16.6, and 21.1 Torr, for each cycle, respectively. A detailed description of the transmission IR cell and experimental setup can be found elsewhere.[19]

Both L-N_2 and L-He were used to cool the sample. The sample was heated to 133 K when L-N_2 was used in the IR cell Dewar flask. Liquid-He was used to achieve lower temperatures by transferring it from a L-He Dewar flask to the IR cell Dewar flask via an evacuated double-walled transfer tube. Helium evaporated at the outlet of the transfer tube, due to poor insulation, producing a cold gas at ∼28 K. The sample was heated to 36 K to avoid temperature fluctuations.

CF_4 (Aldrich Chemical Co., 99.9% purity) was dosed into the IR cell from the gas line. The highest possible pressure of a gas in the IR cell is defined by the sublimation pressure at the coldest point in the system, which is the Dewar flask. When L-N_2 was used as a refrigerant, the saturation pressure was 0.033 Torr, and it was less than 10^{-5} Torr when He was used. For the higher temperature (L-N_2), gas dosed into the IR cell quickly reached a steady state, giving an effective equilibrium between the gas in the cell at a pressure of 0.033 Torr and the gas adsorbed on the nanotubes at 133 K. In contrast, when He was used as a refrigerant, gas dosed into the cell rapidly condensed on both the Dewer flask (at ∼28 K) and the sample (36 K). The mobility of the condensed CF_4 molecules at these low temperatures was extremely low, so that steady state was not achieved over the time of the experiment. An unknown fraction of each dose of CF_4 gas adsorbed on the sample and a constant increase of condensed CF_4 on the sample were observed with each dose. Hence, the L-N_2 experiments could only produce a low coverage of CF_4 on the nanotubes, due to desorption of the gas from the sample, while the low temperature experiments produced macroscopically thick layers of CF_4 adsorbed on the sample.

Transmission IR spectra were measured with a Mattson Research Series FTIR spectrometer equipped with a wide band MCT detector. All spectra were recorded at 4 cm^{-1} resolution with 500 scans for averaging.

IV. Results and Discussion

A. LO−TO Splitting in Bulk CF_4. Our main goal is to determine if LO−TO splitting can occur in confined systems,

(47) Sataty, Y. A.; Ron, A.; Herbstein, F. H. *J. Chem. Phys.* **1975**, *62*, 1094.
(48) Dewhurst, J. K.; Ahuja, R.; Li, S.; Johansson, B. *Phys. Rev. Lett.* **2002**, *88*, 075504.
(49) Kohn, W.; Meir, Y.; Makarov, D. E. *Phys. Rev. Lett.* **1998**, *80*, 4153.
(50) Milet, A.; Korona, T.; Moszynski, R.; Kochanski, E. *J. Chem. Phys.* **1999**, *111*, 7727.
(51) Wu, X.; Vargas, M. C.; Nayak, S.; Lotrich, V.; Scoles, G. *J. Chem. Phys.* **2001**, *115*, 8748.
(52) van Mourik, T.; Gdanitz, R. J. *J. Chem. Phys.* **2002**, *116*, 9620.
(53) Kamiya, M.; Tsuneda, T.; Hirao, K. *J. Chem. Phys.* **2002**, *117*, 6010.
(54) Wesolowski, T. A.; Morgantini, P. Y.; Weber, J. *J. Chem. Phys.* **2002**, *116*, 6411.
(55) Rydberg, H.; Jacobson, N.; Hyldgaard, P.; Simak, S. I.; Lundqvist, B. I.; Langreth, D. C. *Surf. Sci.* **2003**, *532*, 606.
(56) Hesselmann, A.; Jansen, G. *Chem. Phys. Lett.* **2003**, *367*, 778.
(57) Misquitta, A. J.; Jeziorski, B.; Szalewicz, K. *Phys. Rev. Lett.* **2003**, *91*, 033201.
(58) Xu, X.; Goddard, W. A. *J. Chem. Phys.* **2004**, *121*, 4068.
(59) Xu, X.; Goddard, W. A. *Proc. Natl. Acad. Sci. U.S.A.* **2004**, *101*, 2673.
(60) Girifalco, L. A.; Hodak, M. *Phys. Rev. B* **2002**, *65*, 125404.
(61) Zhao, J.-J.; Buldum, A.; Han, J.; Lu, J. P. *Nanotechnology* **2002**, *13*, 195.
(62) Wyckoff, R. W. G. *Crystal Structures*; John Wiley & Sons: New York, London, 1963; Vol. 1.
(63) Wyckoff, R. W. G. *Crystal Structures*; John Wiley & Sons: New York, London, 1964; Vol. 2.
(64) Gonze, X.; Lee, C. *Phys. Rev. B* **1997**, *55*, 10355.
(65) Mawhinney, D. B.; Naumenko, V.; Kuznetsova, A.; Yates, J. T., Jr.; Liu, J.; Smalley, R. E. *J. Am. Chem. Soc.* **2000**, *122*, 2383.

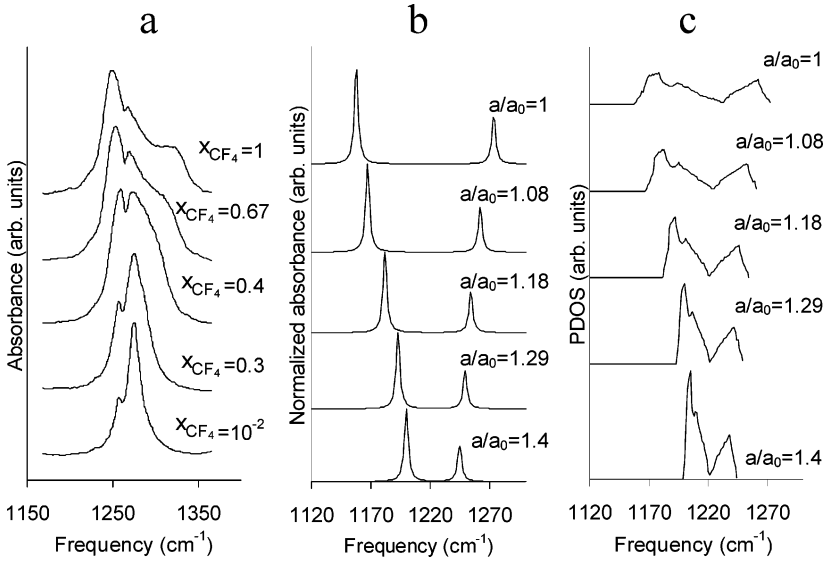

Figure 1. LO−TO splitting of bulk CF_4 as a function of concentration. (a) Experimental Raman spectra for CF_4 dissolved in Ar at different mole fractions. Data from Nectoux et al.[33] (b) The IR absorption for bcc CF_4 computed from density functional perturbation theory as a function of lattice spacing. (c) The computed phonon density of states for bcc CF_4 as a function of lattice spacing.

specifically 1D, quasi-1D, and 2D systems. We first show that our IR absorption and PDOS calculations reliably predict the behavior of bulk CF_4. Nectoux et al. have measured the Raman spectra of CF_4 dissolved in argon at mole fractions ranging from 10^{-2} to 1.[33] At low concentrations, the CF_4 molecules are well separated and the Raman spectrum does not display any LO−TO splitting, as seen from the data in Figure 1a, bottom curve. The LO−TO splitting develops gradually as the concentration of CF_4 increases, as seen by comparing the curves in Figure 1a. A very similar trend can be seen from the LDA/NCPP calculations, presented in Figure 1b and c. The computed IR absorption spectra of the ν_3 mode for bulk CF_4 in a bcc lattice are shown in Figure 1b. The lattice spacing was varied from $a/a_0 = 1.4$ to 1, where a_0 is the equilibrium lattice spacing. At the largest lattice spacing (bottom curve in Figure 1b), the TO and LO peaks are located at 1200 and 1245 cm^{-1}, respectively, giving a splitting of 45 cm^{-1}. The calculated splitting at the equilibrium lattice spacing (top curve in Figure 1b) is 116 cm^{-1}, as compared to the experimental value of 65 cm^{-1} (top curve, Figure 1a). Thus, the magnitude of the splitting computed from DFPT is about twice that observed in experiments, but the trends from the calculations are in qualitative agreement with experiments (compare Figure 1a and b). Note that the experimental Raman spectra show a peak at about 1258 cm^{-1} that is due to Fermi resonance with the first overtone of the ν_4 mode; this effect is not included in the calculations.

Phonon density of states computed for bulk CF_4 as a function of lattice spacing is presented in Figure 1c. The intensity of PDOS is not directly proportional to the IR/Raman intensity because the former involves the vibrational motions at different values of the wave vector ***k*** over the entire first Brillouin zone. In contrast, the IR and Raman intensities result from vibrational motions at the Γ point of the first Brillouin zone. Therefore, the PDOS is not a direct measure of the observable LO−TO splitting in experiments, but it does provide additional information on CF_4 vibrations. We see that the PDOS develops in a way that is qualitatively similar to the experimental Raman spectra as the concentration of CF_4 is increased, either through decreasing the lattice constant (Figure 1c) or through increasing

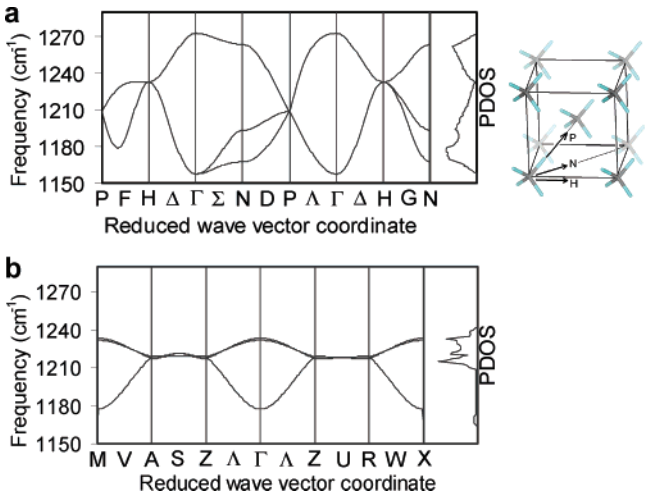

Figure 2. (a) Phonon dispersion curves for bulk CF_4 (body-centered cubic lattice). (b) Phonon dispersion curves for 1D CF_4 packed along the molecular C_3 axis.

the mole fraction (Figure 1a). As stated above, the low-temperature structure of CF_4 is $C2/c$. We have used a bcc lattice in the calculations presented in Figure 1 for computational efficiency. We have computed the PDOS for the $C2/c$ crystal structure and have found that the results are very similar, in accord with the experimental observation that the Raman spectra of CF_4 in the solid and liquid phases are very similar, both exhibiting LO−TO splitting.[32]

Phonon dispersion relations can provide additional insight into LO−TO splitting. The calculated phonon structure of bulk bcc CF_4 (Figure 2a) shows that the TO modes are doubly degenerate at the Γ points (lower frequency) and that the LO mode is nondegenerate (higher frequency). The band valley at 1233 cm^{-1} in the PDOS is due to the dispersion at **H** (0.0, 1.0, 0.0), where the coordinates of the k point in real space are reported in the parentheses. The vibrational motion is triply degenerate at the two special k points, **H** (0.0, 1.0, 0.0) and **P** (0.5, 0.5, 0.5). This is because these two k points are at the vertices of the first Brillouin zone, at which the vibrational

Table 2. ν_3 Vibrational Frequencies of CF_4 in 1D Chains[a]

vibrational mode	M1 (along the packing axis)	M2 (perpendicular to the packing axis)	
LDA/NCPP ($z = 4.4$ Å)	1177 (−41)	1232 (14)	1233 (15)
LDA/USPP ($z = 4.4$ Å)	1188 (−50)	1242 (4)	1245 (7)
LDA/USPP ($z = 4.9$ Å)	1207 (−31)	1239 (1)	1241 (3)
LDA/USPP (10,10) groove	1204 (−34)	1227 (−11)	1243 (5)
LDA/USPP (17,0) groove	1185 (−53)	1234 (−4)	1246 (8)
LDA/USPP (10,10) inside	1204 (−34)	1234 (−4)	1230 (−8)
LDA/USPP (17,0) inside	1186 (−52)	1241 (3)	1237 (−1)

[a] The LDA/NCPP results were computed from DFPT at the Γ point. The LDA/USPP calculations utilized the direct force constant approach. The first three calculations are for isolated 1D chains. The bottom four rows are for CF_4 molecules in groove or internal sites in either (10,10) or (17,0) SWNTs. In all cases, the CF_4 molecules are packed along their C_3 symmetry axis. The vibrational shifts from the gas-phase frequency (from Table 1) are shown in parentheses for each mode.

motions of CF_4 are totally out-of-phase, resulting in the absence of LO−TO splitting.

The phonon dispersion relations (Figure 2a) indicate that the TO band depends on the intralayer and interlayer CF_4 interactions. The inset in Figure 2a shows the special k point directions relative to the bcc lattice. The phonon at **N** (0.5, 0.5, 0.0) contributes to the PDOS intensity around 1168 and 1193 cm^{-1}; the phonon dispersion from **P** (0.5, 0.5, 0.5) to **H** (0.0, 1.0, 0.0) contributes to the PDOS intensity around 1179 cm^{-1}. For the TO dispersion long **P**−**H**, there exists a minimum in the phonon dispersion curves located at the k point (0.35, 0.65, 0.35), which is almost parallel to the direction of the C−F bond pointing from one (110) layer to another. Moving from **P** to **H**, the dynamic dipole is not canceled out and the dipolar interaction leads to TO coupling between different layers. As shown in the inset of Figure 2a, the plane spanned by Γ−**P** and Γ−**N** is parallel to the (110) CF_4 layer, and the phonon dispersion along **P**−**H** is pointing out of the (110) layer. So these intralayer and interlayer phonon interactions result in the TO band in the PDOS spectra. The phonon dispersion along Γ−N contributes to the PDOS of the LO band around 1261 cm^{-1}. The IR absorption and PDOS calculations presented here represent, to our knowledge, the first example of LO−TO splitting for molecular solids computed from first principles.

B. One-Dimensional Systems. We have computed vibrational frequencies from the direct force constant approach to complement the IR intensity and PDOS of calculations to study vibrational modes in 1D chains of CF_4 molecules. The ν_3 vibrational frequencies calculated from LDA/USPP and LDA/NCPP for linear CF_4 chains are summarized in Table 2, and the corresponding vibrational motions are schematically illustrated in Figure 3. Lattice parameters of 4.4 and 4.9 Å were used; the former corresponds to the optimized 1D structure for CF_4 aligned along the C_3 axis, and the latter is the lattice spacing for two primitive unit cells of a (10,10) SWNT. Comparing the ν_3 frequencies in Tables 1 and 2, we see that one of the modes is red-shifted (softened) and two modes are blue-shifted (hardened) for molecules in the 1D chain as compared to the gas phase. The frequency shift from the gas phase for each mode is given in parentheses in Table 2. The shifting of the frequencies in the 1D chain is consistent with LO−TO splitting. The in-phase C−F stretching along the packing axis softens the ν_3 mode (M1 in Figure 3a and Table 2), while the C−F stretching perpendicular to the packing axis hardens the ν_3 mode (M2 in Figure 3b and Table 2). Both LDA/ NCPP and LDA/USPP show the same trends. Similar results were obtained for a linear CO_2 chain,[41] where the asymmetric CO_2 stretching mode is softened as compared to the gas-phase value. The softening of the modes can be explained by the electrostatic interaction between the dynamic dipoles (Figure 3a), where the dynamic dipoles are parallel to the electric field lines. The in-phase stretch is therefore energetically stabilized. For the ν_3 vibrations perpendicular to the packing axis, the dynamic dipole generates an opposing electric field on the neighboring dynamic dipole (Figure 3b), leading to mode hardening. Our calculations predict that the LO−TO splitting in a 1D chain is between 30 and 55 cm^{-1}. Taking the convention that the softened mode is the TO mode, there is one TO mode and two nearly degenerate LO modes for a linear chain of CF_4 molecules. We note that the LO modes are only weakly blue-shifted, with shifts ranging from 1 to 15 cm^{-1}. In contrast, the mode in the TO region is shifted by about 30−50 cm^{-1}, with the larger red-shift corresponding to the smallest lattice spacing. Hence, the LO−TO splitting is qualitatively different in a 1D chain as compared to the bulk, where the LO modes are blue-shifted by 56 cm^{-1} and the TO modes are red-shifted by 60 cm^{-1}. We note that results from LDA/NCPP and LDA/USPP calculations are in quantitative agreement.

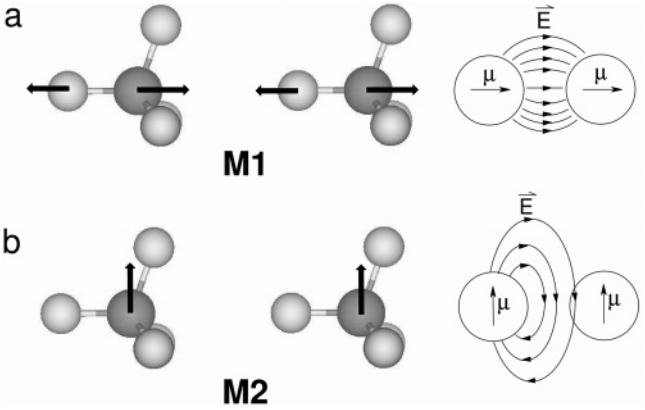

Figure 3. Schematic diagram of the interactions between the dynamic dipoles at the Γ point. (a) ν_3 vibration along the packing axis; (b) ν_3 vibrations perpendicular to the packing axis.

The previous calculations considered 1D chains of CF_4 molecules in free space. In reality, the molecules are adsorbed in SWNT groove and internal adsorption sites. The ν_3 vibrational frequencies for a 1D chain of CF_4 in the groove and internal sites of both (10,l0) and (17,0) SWNTs are shown in Figure 4 and Table 2. Only the frequencies have been computed because the number of atoms in the supercells of these systems precluded IR intensity and PDOS calculations. We see from Table 2 that the M1 modes for molecules in the groove site and inside the nanotubes have about the same red-shifts (34−53 cm^{-1}) as molecules in a 1D chain without the nanotube. However, the M2 modes for molecules in groove and internal sites are no longer all blue-shifted. Five of the M2 modes are slightly red-shifted (1−11 cm^{-1}), and three modes are blue-shifted by a small amount (3−8 cm^{-1}). We also note that the TO mode for CF_4 on the (17,0) tube is more strongly red-shifted than that on the (10,10), both for groove and for internal sites. This is because the lattice spacing along the tube axis is substantially smaller for the (17,0) tube, giving stronger CF_4−CF_4 coupling. The

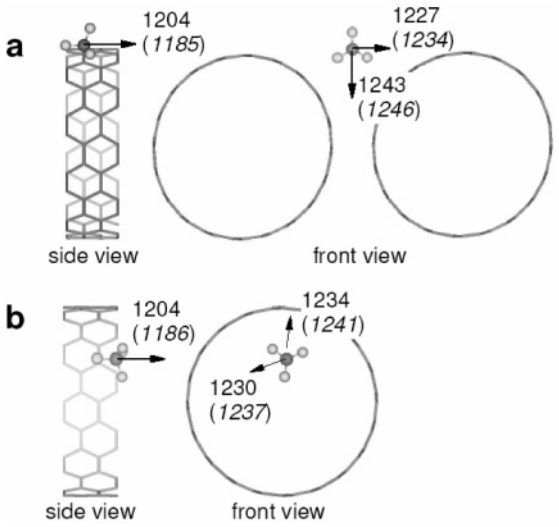

Figure 4. ν_3 vibrational modes of CF_4 calculated from VASP. (a) CF_4 in the groove site; (b) CF_4 on the SWNT interior site. The vibrational frequencies are given in cm^{-1}. The numbers without parentheses are for CF_4/(10,10) SWNT. The numbers in parentheses are for CF_4/(17,0) SWNT.

results for the vibrational calculations are qualitatively similar for CF_4 adsorbed on the (10,10) and (17,0) nanotubes, when the differences in the lattice spacing are taken into account. This indicates that the conductivity of the nanotube does not have a substantial effect on the vibrational modes of a weakly adsorbed species. The overall effect of the nanotubes on the ν_3 modes is to reduce the blue-shift of the M2 modes, while leaving the M1 mode virtually unchanged. Groove site adsorption for both the (10,10) and the (17,0) nanotubes splits the near-degeneracy of the M2 modes as compared to the isolated 1D chains and chains adsorbed inside the nanotubes. Thus, while it can be said that LO−TO splitting does occur for 1D chains in both free space and in nanotubes, the character and magnitude of the splitting are very different from that observed in the bulk.

The best comparison between calculated and experimental IR spectra would be for realistic geometries of CF_4 molecules adsorbed on the groove and internal sites of $SWNT_S$. Unfortunately, the linear response calculation using PWscf is prohibitively difficult for such systems. We have therefore attempted to mimic the effect of concentration and packing geometry by performing LDA/NCPP calculations for the IR absorbance for a linear chain of CF_4 molecules varying the distance between the molecules, and by considering CF_4 molecules packed into a zigzag geometry. The former calculations mimic the effect of low coverages of CF_4 molecules in the groove site, as observed from classical Monte Carlo simulations.[19] The latter calculations model the effects of nonlinear packing of CF_4 molecules inside the nanotubes, also observed in classical adsorption simulations.[19]

The IR absorbance for a single chain of CF_4 molecules at different values of the distance between the molecules is plotted in Figure 5. The CF_4 molecules are packed along the C_3 axis, although similar results are observed for packing along the C_2 axis. The distance between the molecule centers is given for each curve. The top curve is for a close-packed optimized structure, where the molecules are 4.4 Å apart. Note that the LO−TO splitting is about 55 cm^{-1} for the close-packed structure and that the splitting decreases to about 18 cm^{-1} when the CF_4 molecules are spaced 7.0 Å apart. The close-packed splitting

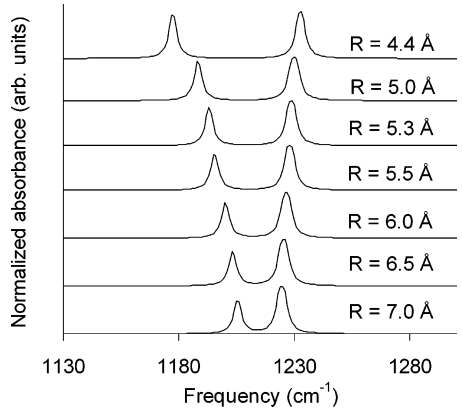

Figure 5. Computed IR absorbance for a 1D in-line chain of CF_4 molecules aligned along their C_3 axes. The lattice spacing increases from the top curve to the bottom curve with the spacing, *R*, shown on each curve.

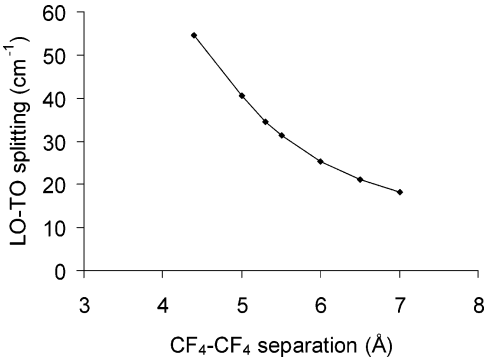

Figure 6. The calculated LO−TO splitting as a function of the CF_4−CF_4 separation for the 1D chain IR spectra shown in Figure 5.

in 1D is less than one-half the splitting calculated for the bulk bcc phase of about 116 cm^{-1} (see Figure 1). The LO−TO splitting as a function of CF_4 separation is plotted in Figure 6. It is obvious from this plot that the splitting drops dramatically with an increase in nearest-neighbor distance. The average nearest-neighbor distance for CF_4 molecules adsorbed inside the nanotubes at the experimental conditions of 133 K and 0.033 torr is about 5.3 Å, as determined from Monte Carlo simulations.[19] This average spacing would result in LO−TO splitting of about 35 cm^{-1} according to Figure 6. The splitting observed experimentally in bulk CF_4 is 65 cm^{-1},[33] roughly one-half that predicted in our calculations. If the splitting is overestimated in all of our calculations, then the 1D chains with neighboring CF_4 distances greater than about 5.5 Å may not appear to have LO−TO splitting because the two peaks would be merged. This implies that it would not be possible to observe LO−TO splitting from CF_4 adsorbed in the groove sites, because the concentration of molecules is predicted to be quite low.[19]

We have computed the PDOS and phonon dispersion relations for the 1D linear chain geometry as a complement to the IR absorbance calculations. From Figure 2b, it can be seen that LO−TO splitting does indeed occur for the linear CF_4 chain at the Γ point; the splitting is evident from the spread between the low-frequency band and the two high-frequency bands near the Γ point. The Γ−**Z** direction in Figure 2b points along the chain axis. Note that the high-frequency LO mode is composed of two nearly degenerate bands, in agreement with both the IR frequency and the absorption calculations. The most striking feature of Figure 2b is that the PDOS is very low around the

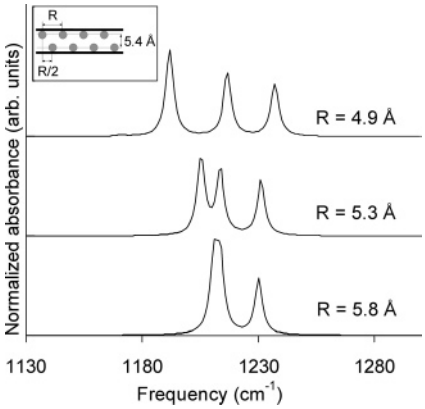

Figure 7. Calculated IR absorbance for a 1D zigzag chain of CF_4 molecules. The lattice spacing along the chain axis is increased from the top curve to the bottom curve.

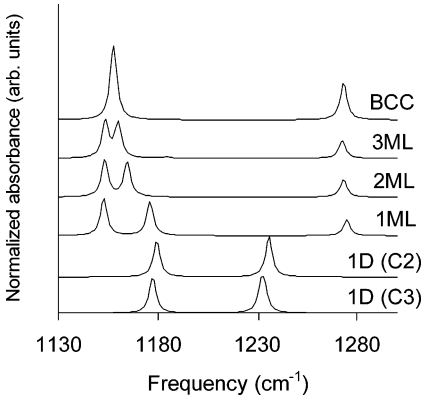

Figure 8. Calculated IR absorption spectra. From top to bottom: (a) bulk CF_4 (bcc lattice); (b) 3 ML CF_4; (c) 2 ML CF_4; (d) 1 ML CF_4; (e) 1D CF_4 packed along the molecular C_2 axis; and (f) 1D CF_4 packed along the molecular C_3 axis.

TO region, at about 1180 cm^{-1}, as can be seen by comparing the PDOS curve on the right axis of Figure 2b with the dispersion curve. The low PDOS in the TO region does not translate into low IR absorbance, as can be seen from Figure 5, where the TO absorption is about equal to that of the LO mode.

The 1D chain is a reasonable approximation for the geometry of molecules adsorbed in the groove sites. Model calculations have shown that CF_4 molecules adsorbed inside SWNTs adopt a geometry that is closer to a zigzag 1D chain. The IR absorbance of CF_4 molecules confined to a zigzag configuration is plotted in Figure 7. The geometry of the 1D zigzag chain is shown in the inset of Figure 7. The heavy lines represent the wall of the nanotube. The two length scales defining the geometry are also shown in Figure 7. The distance perpendicular to the zigzag axis was held fixed at 5.4 Å, while the distance between molecules along the axis was varied from a close-packed distance of 4.9 to 5.8 Å. The zigzag structure gives a simulated IR spectrum containing three peaks, one TO peak at about 1190 cm^{-1}, a LO peak at about 1240 cm^{-1}, and a gas-phase-like peak at 1217 cm^{-1}. The two peaks at lower frequency quickly merge with increasing CF_4-CF_4 distance, as can be seen from the bottom curve in Figure 7. These calculations for the zigzag phase agree with the pure 1D chain calculation in that the LO−TO splitting decreases rapidly with increased adsorbate−adsorbate spacing. The zigzag phase, however, indicates that additional peaks will occur for off-axis packing, possibly giving rise to broadening. These features would serve to mask the appearance of the LO−TO modes in experiments.

C. LO−TO Splitting in 1D, 2D, and 3D. In this section, we compare IR absorption spectra for CF_4 in 1D chains, in 2D structures (monolayer and multilayers), and in the 3D bulk crystal. The calculated spectra are given in Figure 8. We have normalized the intensity in all of the absorption calculations so that the number of CF_4 molecules being irradiated is the same in different structures. Note that this is different from experiments where higher coverages will lead to a larger IR signal according to Beer's law. The LO−TO peaks are not sensitive to the relative orientation of adjacent CF_4 molecules because CF_4 packed along its C_2 axis and along its C_3 axis show similar results.

The 2D structures have two TO modes and one LO mode, in contrast to the 1D chains, which have one TO mode and two LO modes. The calculated IR spectra clearly show that the two TO modes are split in the monolayer (1 ML curve) and that the two peaks merge as the number of layers increase (2 ML and 3 ML curves in Figure 8). The splitting is due to anisotropy in the 2D structure. The TO mode in the bulk (bcc curve in Figure 8) is doubly degenerate. The absorption intensity grows slowly from 1 ML, 2 ML, to 3 ML. The TO band has a larger intensity because there are two TO modes and one LO mode; that is, the absorbance ratio is about 2:1 for TO:LO in the bulk.

The ν_3 vibrations parallel to the slab have lower frequencies, analogous to the vibrational mode aligned along the 1D chain; it follows that the 2D geometry has two TO modes because there are two in-plane directions. For the ν_3 mode in the out-of-plane direction, the dynamic dipoles are coupled repulsively to their nearest neighbor, giving a shift to higher frequency, analogous to the motions shown in Figure 3b. Hence, one of the LO modes becomes a TO mode in going from 1D to 2D. One of the LO modes in 1D gradually becomes a TO mode as lines of 1D chains are brought together to form a 2D slab. There is also another qualitative difference in the LO−TO splitting between 1D and 2D systems. The LO mode in 1D is only slightly blue-shifted, whereas it is strongly blue-shifted in the 2D and 3D systems, as can be seen by comparing the curves in Figure 8.

The PDOS for the systems shown in Figure 8 are presented in Figure 9. The PDOS for 1D chains packed along the C_3 and C_2 axis are shown in Figure 9 as curves f and e, respectively. The PDOS are qualitatively similar for both packings; both show a very low density of states in the TO region and a considerably higher density of states in the LO region, with a broad plateau region of low PDOS separating the two. In going from 1D to 2D (Figure 9d), we see that the LO PDOS is decreased and the PDOS in the TO region is increased and broadened.

The change in lattice dynamics due to adding a second layer to the 2D monolayer can be seen by comparing Figure 9d and c. A new characteristic peak appears at 1191 cm^{-1}, corresponding to layer−layer interactions. This characteristic peak is between the LO band, which ranges from 1230 to 1253 cm^{-1}, and the small TO shoulder at 1172 cm^{-1}. The PDOS at the TO band becomes larger as the number of layers is increased, as can be seen by comparing curves d, c, and b in Figure 9, which correspond to the monolayer, bilayer, and trilayer, respectively. The PDOS of the 2D structures become increasingly like the PDOS of the bulk CF_4, shown in Figure 9a, as the number of layers is increased.

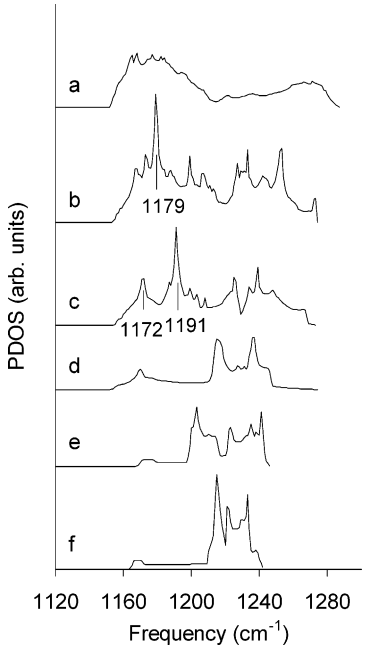

Figure 9. (a) PDOS of bulk CF_4 in *C*2/*c* structure; (b) PDOS of 3 ML of CF_4; (c) PDOS of 2 ML of CF_4; (d) PDOS of 1 ML of CF_4; (e) PDOS of CF_4 in a linear chain packed along the molecular C_2 axis; and (f) PDOS of 1D CF_4 packed along the molecular C_3 axis.

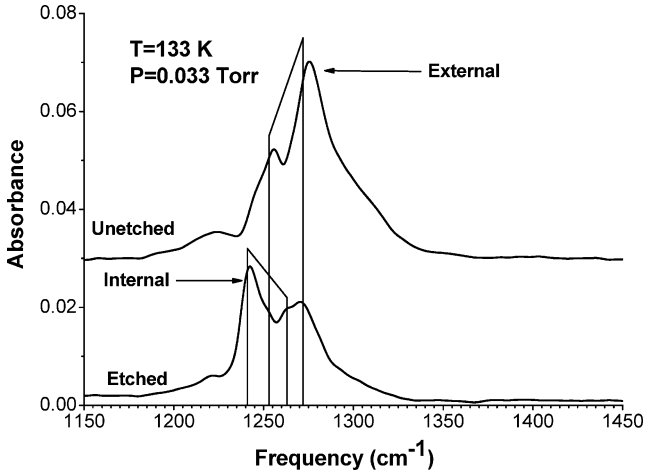

Figure 10. Experimentally measured IR spectra for CF_4 adsorbed on SWNTs at 133 K and a pressure of 0.033 Torr.

D. Experimental Results. Figure 10 shows the IR spectra of CF_4 adsorbed at 133 K and 0.033 Torr on etched and unetched SWNTs. A doublet with peaks at 1253 and 1272 cm^{-1} is observed in the spectrum of CF_4 adsorbed on the unetched SWNTs. This results from the Fermi resonance of the fundamental ν_3 mode and the first overtone of the ν_4 mode. The ν_4 overtone is not included in any of the calculations. The more intensive ν_3 mode is located in the higher frequency range relative to the overtone of the ν_4 mode. The frequencies of these bands can be extracted by the Fermi self-deconvolution method described previously[19] and are located at 1267 and 1257 cm^{-1}, respectively, for the ν_3 fundamental and the first overtone of ν_4 mode. This doublet is assigned to CF_4 molecules adsorbed in the groove sites of SWNT bundles.

The internal sites become available for adsorption upon etching of the SWNTs. The IR spectrum of CF_4 on the etched tubes has a doublet with peaks at 1263 and 1241 cm^{-1} in addition to the doublet observed for the unetched SWNTs. This doublet is assigned to CF_4 adsorbed in the nanotube interior. On the basis of the intensity ratio, the fundamental ν_3 mode is believed to be shifted greater than the overtone and is located in the lower frequency region. The Fermi self-deconvolution analysis gives the frequencies of the ν_3 and $2\nu_4$ modes at 1247 and 1258 cm^{-1}, respectively. Adsorption in the nanotube interior is accompanied by stronger adsorbate−adsorbent interaction due to the deeper potential well inside of the nanotubes. This caused softening of vibration motion and higher red-shift of the band. The degree of softening depends on the transition dipole moment that is much greater for the ν_3 mode than for the $2\nu_4$ mode; therefore, the ν_3 mode is more red-shifted.

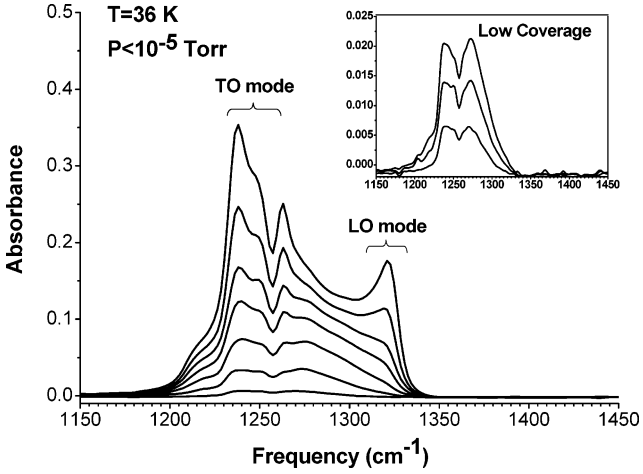

Figure 11. Experimentally measured IR spectra for CF_4 adsorbed on SWNTs at 36 K. The coverage is increased from the bottom curve to the top.

Figure 11 shows the IR spectra of CF_4 adsorbed on etched SWNTs at 36 K. At low coverages, the spectral profile resembles the profile of IR spectra of CF_4 adsorbed at 133 K; two families of peaks are observed that may be attributed to overlapping of two doublets observed at higher temperatures. However, as the coverage increases, a peak at ~1239 cm^{-1} starts to appear followed by the development of a less intense and broad shoulder at 1320 cm^{-1} that shifts to higher frequency with increasing coverage. At very high coverages, these two bands are observed at 1238 and 1321 cm^{-1} and can be assigned to TO and LO modes, respectively, detected for condensed phases of CF_4. Thus, CF_4 at low coverages presumably adsorbs in the groove sites and partially inside of nanotubes because the low temperature limits diffusion on the surface. As the coverage increases, larger clusters of CF_4 appear, forming increasingly thick layers on the surface of the SWNTs. The appearance of LO−TO splitting coincides with the increase in CF_4 coverage.

V. Conclusions

We have presented the first set of comprehensive ab initio calculations for LO−TO splitting in systems of differing dimensionality. We have computed vibrational frequencies, IR absorption, and the phonon density of states for CF_4 in one, two, and three dimensions. We have studied how LO−TO modes develop as the dimensionality is changed. There are two LO modes and one TO mode for an in-line 1D chain of CF_4 molecules. In contrast, 2D structures have one LO mode and two TO modes. One of the 1D LO modes becomes an in-plane

TO mode in going from 1D to 2D. The phonon modes for 1D chains and 2D sheets have a relatively low density of states in the TO region. The TO PDOS are developed through interlayer interactions as can be seen by comparing monolayer, bilayer, trilayer, and bulk lattice structures.

We have measured IR spectra of CF_4 adsorbed on samples of unetched and etched SWNTs at 133 K and 0.033 Torr. No LO−TO splitting was observed. We also measured IR spectra at 36 K over a wide range of coverages and found that LO−TO splitting developed gradually as the coverage was increased.

Our calculations demonstrate that LO−TO splitting does, in principle, occur for CF_4 molecules confined to 1D, both in linear and in zigzag chains. The question then is why LO−TO splitting cannot be observed in experiments at low coverages of CF_4 on SWNT samples. The calculations indicate that there are dramatic qualitative differences between LO−TO splitting in 1D and 2D or 3D. Specifically, (1) the splitting is much smaller for 1D and quasi-1D structures at close packing than for the bulk (Figure 8), (2) the LO modes are very weakly blue-shifted, and (3) the nanotubes and packing disorder introduce additional peaks and shift the LO modes to lower frequencies (Table 2 and Figure 7). Therefore, LO−TO splitting for 1D and quasi-1D systems cannot be observed experimentally from the somewhat broad experimental peaks (see Figures 10 and 11). The IR frequencies show that the ν_3 modes in 1D are red-shifted, but not strongly blue-shifted. When the nanotubes are included in the frequency calculations, the blue-shifted frequencies almost entirely disappear (Table 2). This is in qualitative agreement with the experiments, which show absorption in the red-shifted region but not at higher frequencies at low coverages (Figure 11, inset). The LO peak observed in the IR absorption and PDOS calculations shifts to higher frequencies as the coverage increases from 1D to 2D (Figures 8 and 9). This is also in qualitative agreement with experiments (Figure 11).

We note that the computed LO−TO splitting for bulk CF_4 is too large as compared to experiments by about a factor of 2. This is likely the result of inaccuracy of the exchange-correlation functional. We performed limited calculations with two different generalized gradient approximations, PBE[66] and PW91,[67] but the results were not an improvement over the LDA calculations. We assume that the LO−TO splitting in all of our calculations is overpredicted. Therefore, the true splitting in 1D systems could be much smaller than our calculations indicate, giving another reason for the lack of observed LO−TO splitting in the experiments.

Note that we have only included a single CF_4 molecule in the supercell of most of our calculations and we have ignored the effect of the nanotube on the IR absorption and PDOS. Inclusion of multiple CF_4 molecules would have allowed us to investigate orientational and packing effects that are lacking in this study. These effects may have given us a better understanding as to why LO−TO splitting is absent in the experiments. Nevertheless, there is enough qualitative agreement between experiments and calculations to allow us to conclude that, while LO−TO splitting is formally present in 1D systems, in practice it cannot be observed.

The calculated PDOS for 1D, 2D, and 3D structures show substantial differences, as can be seen from Figure 9. The density of states in the TO region is very small for 1D and 2D monolayer structures. The PDOS in the TO region increase dramatically with the addition of mutilayers, while the LO PDOS both increase and shift to higher frequencies. These theoretical predictions should be tested experimentally by inelastic neutron scattering.

We propose that LO−TO splitting can be used as a sensitive marker for identifying one-dimensional states of matter. The qualitative changes in the vibrational spectrum and PDOS for CF_4 as a function of dimensionality make the ν_3 mode an excellent probe of the effective dimensionality of adsorbed molecules. Our results agree with those of Devlin et al., who have previously proposed the use of ν_3 spectroscopy as a probe for 2D surface structure.[34,35] It should be possible to use other molecules that display LO−TO splitting, such as CCl_4, HCN,[68,69] or *meta*-nitroaniline[70] as probes of the effective dimensionality of an environment.

Acknowledgment. We gratefully acknowledge the Army Research Office for support of this work. Computations were performed at the Center for Molecular and Materials Simulations at the University of Pittsburgh and at the U.S. Army Research Laboratory Major Shared Resource Center through a Department of Defense High Performance Computing challenge grant.

JA043540V

(66) Perdew, J. P.; Burke, K.; Ernzerhof, M. *Phys. Rev. Lett.* **1996**, *77*, 3865.
(67) Perdew, J. P. PW 91 functionals. In *Electronic Structure of Solids*; Ziesche, P., Eschrig, H., Eds.; Akademie Verlag: Berlin, 1991; p 11.
(68) Muller, B.; Lutz, H. D.; Hermeling, J.; Knozinger, E. *Spectrochim. Acta. Part A* **1993**, *49*, 191.
(69) Aoki, K.; Baer, B. J.; Cynn, H. C.; Nicol, M. *Phys. Rev. B* **1990**, *42*, 4298.
(70) Szostak, M. M.; Lecalve, N.; Romain, F.; Pasquier, B. *Chem. Phys.* **1994**, *187*, 373.